CuZn Superoxide Dismutase Geometry Optimization, Energetics, and Redox Potential Calculations by Density Functional and Electrostatic Methods

Robert Konecny,*,† Jian Li, Cindy L. Fisher,‡ Valerie Dillet, Donald Bashford, and Louis Noodleman*

Department of Molecular Biology, TPC-15, The Scripps Research Institute, La Jolla, California 92037

Received June 25, 1998

The structures, energetics, and orbital- and charge-dependent properties of copper zinc superoxide dismutase (CuZnSOD) have been studied using density functional and electrostatic methods. The CuZnSOD was represented with a model consisting of copper and zinc sites connected by a bridging histidine ligand. In addition to the bridge, three histidine ligands and one water molecule were bonded to the Cu ion in the copper site as first-shell ligands. Two histidine ligands and an aspartate were coordinated to the zinc ion in the zinc site. Full optimization of the model was performed using different functionals, both local and nonlocal. Geometrical parameters calculated with the nonlocal functionals agree well with the experimental X-ray data. In our calculated results, the His61 Nϵ−Cu bond in the active site breaks during the reduction and protonation, consistent with a number of X-ray structures and with EXAFS and NMR evidence. The reduction potential and pK_a of the coupled electron/proton reaction catalyzed by CuZnSOD were determined using different models for the extended environment—from an electrostatic representation of continuum solvent, to the full protein/solvent environment using a Poisson−Boltzmann method. The predicted redox potential and pK_a values determined using the model with the full protein/solvent environment are in excellent agreement with experiment. Inclusion of the full protein environment is essential for an accurate description of the redox process. Although the zinc ion does not play a direct redox role in the dismutation, its electronic contribution is very important for the catalytic mechanism.

1. Introduction

Superoxide dismutases (SODs) are a diverse group of metalloenzymes whose role is the catalytic dismutation of two negatively charged superoxide radicals to molecular oxygen and hydrogen peroxide. The biological functions of SODs are very important—they prevent oxidative damage and inflammation due to toxic oxygen intermediates and are involved in anticancer and antiaging mechanisms.[1,2,4]

The only class of SODs where the active site contains two different metal ions is a family of copper zinc superoxide dismutases (CuZnSODs). The CuZnSOD is a dimeric protein where the two identical subunits are noncovalently bonded.[1] Each subunit contains one copper(II) and one zinc(II) ion in the oxidized ("resting") state. During catalysis, copper is the redox partner of the superoxide radical, whereas the oxidative state of Zn^{2+} does not change during the dismutation reaction. The interaction between the two subunits in the dimer is probably not important for the catalytic process since there is a large distance between the two remote copper sites (∼34 Å).

The copper(II) and zinc(II) in each subunit in the oxidized form of CuZnSOD are connected by a histidine imidazolate bridge (His61; numbering of bovine erythrocyte CuZnSOD) (Figure 1). The Cu^{2+} ion is coordinated by ϵ nitrogen atoms of His46, His61, and His118 and the Nδ of His44 (and more distantly by a water molecule) in a square planar geometry with tetrahedral distortion. The zinc(II) site has the geometry of a distorted tetrahedron created by three Nδ-coordinated histidines and an aspartate residue: His61, His69, His78, and Asp81. The bridging ligand His61 lies nearly on a straight line between Cu^{2+} and Zn^{2+}, which are separated by 6 Å.

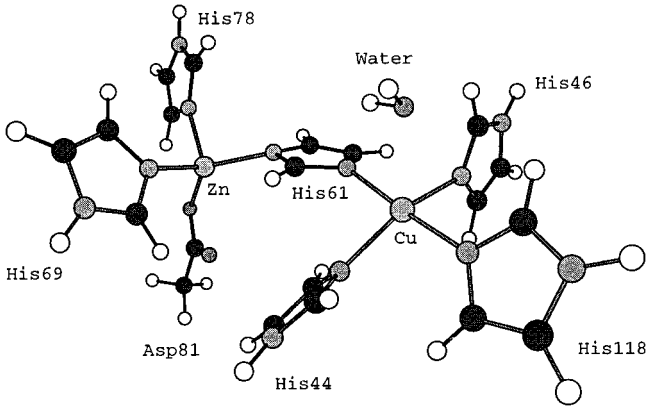

Figure 1. Schematic representation of the active site in the oxidized CuZnSOD (ligand numbering corresponding to numbering of bovine erythrocyte CuZnSOD).

The active-site Cu^{2+} ion is at the bottom of a deep and narrow (<4 Å) channel in the protein, while the Zn^{2+} ion is completely buried. There is no evidence that the potential ligands can bind

† Current address: Department of Chemistry, Baker Laboratory, Cornell University, Ithaca, NY 14853-1301.

‡ Current address: Structural Bioinformatics, Inc., 10929 Technology Place, San Diego, CA 92127.

(1) Bannister, J. V.; Bannister, W. H.; Rotilio, G. *CRC Crit. Rev. Biochem.* **1987**, *22*, 111−180.
(2) Holm, R. H.; Kennepohl, P.; Solomon, E. I. *Chem. Rev.* **1996**, *96*, 2239−2314.
(3) Barrette, W. C., Jr.; Sawyer, D. T.; Fee, J. A.; Asada, K. *Biochemistry* **1983**, *22*, 624−627.
(4) Miller, A.-F.; Sorkin, D. L. *Comments Mol. Cell. Biophys.* **1997**, *9*, 1−48.

10.1021/ic980730w CCC: $18.00
Published on Web 02/12/1999

to the zinc center; rather, the Zn^{2+} ion appears to play both a structural role and a role in electronic polarization and electrostatic stabilization. While the Zn^{2+} ion is not directly involved in the catalytic process, it probably participates in the catalysis indirectly by interacting with the Cu center and the His61 bridge. The positively charged copper and zinc atoms in the active site, together with other positively charged residues, form a region of strong positive potential which attracts the superoxide to the copper. The binding of the superoxide to the Cu^{2+} center may be also assisted by a positive arginine residue (Arg141) which is located about 5 Å from the Cu^{2+} ion.[5−8]

Mechanistic studies using pulse radiolysis established that the copper center is catalytically reduced and oxidized by superoxide in two steps.[9,10] Superoxide first reduces the Cu^{2+} ion to form dioxygen, and then another molecule of superoxide oxidizes the Cu^{+} ion to produce hydrogen peroxide. The protons required to form the product are taken from the aqueous medium.[11] The catalytic reactions are nearly diffusion limited, occurring at a specific rate of 2×10^9 M^{-1} s^{-1} at the copper site.[11] The overall mechanism can be summarized as

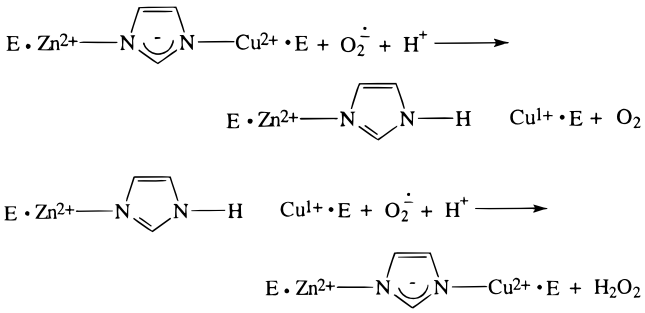

where E symbolizes the rest of the protein.

In the first step, the protonation of the imidazolate bridge in the reduced copper(I) enzyme is accompanied by the dissociation of the His61 Nϵ−Cu bond. This leads to an approximately trigonal planar Cu coordination to three terminal histidines, with the bridging His61 Nϵ−Cu bond being broken. The Zn coordination stays intact, its coordination geometry remaining similar to that in the oxidized form. In the reoxidation step, the His61 donates the proton to the substrate upon oxidation of Cu^{+} to Cu^{2+} and rebinds to Cu^{2+}. Although most experimental observations[12−14] support a model of the reduced CuZnSOD with the His61 Nϵ−Cu bond broken, Wilson et al.[15,16] reported reduced structures where the bond is intact. We will address these structural issues later in section 3. The main kinetic argument against the reduced form with the His61 Nϵ−Cu bond broken is that the reaction rate may be too fast for protonation and deprotonation of the bridging histidine to occur at saturating $O_2^{\bullet-}$ concentrations,[11] and in that case, the active site can only undergo a minor conformational rearrangement. However, if there is only a small energetic barrier to the breaking and forming of the His61 Nϵ−Cu bond, this process may occur, particularly if there is a sufficient flux of protons.

To provide the thermodynamic driving force needed for rapid oxidation and then the reduction of the superoxide anions, the reduction potential of superoxide dismutase must lie within a range spanned by reduction potentials for O_2 and O_2^{-}, between about −0.16 V and +0.89 V.[3] The experimental redox potentials for MnSOD, FeSOD, and CuZnSOD are all almost in the middle of this range.[3] There have been several experimental measurements of the CuZnSOD reduction potential, with the E°_{redox} in the range from +0.310 to +0.420 V[17−19] although Verhagen et al. reported value of +0.102 V[20] versus standard hydrogen electrode (SHE) at pH 7.0. A recent experimentally observed value is +0.403 V.[21]

The catalytic rate of native SOD is pH independent over the pH range 5−9.5.[9,22,23] However, the activity of the Zn-deficient form of the enzyme is pH dependent, which reflects the role of the zinc and the bridging imidazolate in maintaining the copper(II) coordination-sphere configuration and modulating the pK_a of the formerly bridging His61 in the reduced enzyme.[24] The measured pK_a in reduced copper zinc superoxide dismutase is 10.7−10.8.[19,23]

Several molecular dynamics simulation studies have been reported on the dynamics of the active site,[25−27] on its interaction with the substrate (O_2^{-}),[28−30] and on the dynamics of mutants.[31,32] Carloni et al.[30] used the Car−Parrinello projected augmented wave method with local density approximation to study the electron-transfer process between the active site copper(II) ion and superoxide. Their results also support the active role of the Arg141 residue in the catalytic cycle.

In this paper, we investigate the energetics of copper zinc superoxide dismutase throughout its redox cycle using density

(5) Osman, R.; Basch, H. *J. Am. Chem. Soc.* **1984**, *106*, 5710−5714.
(6) Bertini, I.; Lepori, A.; Luchinat, C.; Turano, P. *Inorg. Chem.* **1991**, *30*, 3363−3364.
(7) Djinović Carugo, K.; Battistoni, A.; Carri, M. T.; Polticelli, F.; Desideri, A.; Rotilio, G.; Coda, A.; Bolognesi, M. *FEBS Lett.* **1994**, *349*, 93−98.
(8) Djinović Carugo, K.; Polticelli, F.; Desideri, A.; Rotilio, G.; Wilson, K. S.; Bolognesi, M. *J. Mol. Biol.* **1994**, *240*, 179−183.
(9) Klug-Roth, D.; Fridovich, I.; Rabani, J. *J. Am. Chem. Soc.* **1973**, *95*, 2786.
(10) Fielden, E. M.; Roberts, P. B.; Bray, R. C.; Lowe, D. J.; Mautner, G. N.; Rotilio, G.; Calabrese, L. *Biochem. J.* **1974**, *499*, 139.
(11) Fee, J. A.; Bull, C. *J. Biol. Chem.* **1986**, *261*, 13000−13005.
(12) Blackburn, N. J.; Hasnain, S. S.; Binsted, N.; Diakun, G. P.; Garner, C. D.; Knowles, P. F. *Biochem. J.* **1984**, *219*, 985−990.
(13) Ogihara, N. L.; Parge, H. E.; Hart, P. J.; Weiss, M. S.; Goto, J. J.; Crane, B. R.; Tsang, J.; Slater, K.; Roe, J. A.; Valentine, J. S.; Eisenberg, D.; Tainer, J. A. *Biochemistry* **1996**, *35*, 2316−2321.
(14) Murphy, L. M.; Strange, R. W.; Hasnain, S. S. *Structure* **1997**, *5*, 371−379.
(15) Banci, L.; Bertini, I.; Bruni, B.; Carloni, P.; Luchinat, C.; Mangani, S.; Orioli, P. L.; Piccioli, M.; Ripniewski, W.; Wilson, K. S. *Biochem. Biophys. Res. Commun.* **1994**, *202*, 1088−1095.
(16) Rypniewski, W. R.; Mangani, S.; Bruni, B.; Orioli, P. L.; Casati, M.; Wilson, K. S. *J. Mol. Biol.* **1995**, *251*, 282−296.
(17) Fee, J. A.; DiCorleto, P. E. *Biochemistry* **1973**, *12*, 4893.
(18) Lawrence, G. D.; Sawyer, D. T. *Biochemistry* **1979**, *18*, 3045.
(19) Azab, H. A.; Banci, L.; Bosari, M.; Luchinat, C.; Sola, M.; Viezzoli, M. S. *Inorg. Chem.* **1992**, *31*, 4649−4655.
(20) Verhagen, M. F. J. M.; Meussen, E. T. M.; Hagen, W. R. *Biochim. Biophys. Acta* **1995**, *1244*, 99−103.
(21) St. Clair, C. S.; Gray, H. B.; Valentine, J. S. *Inorg. Chem.* **1992**, *31*, 925−927.
(22) Rotilio, G.; Bray, R. C.; Fielden, E. M. *Biochim. Biophys. Acta* **1972**, *268*, 605−609.
(23) Banci, L.; Bertini, I.; Cabelli, D.; Hallewell, R. A.; Luchinat, C.; Viezzoli, M. S. *Inorg. Chem.* **1990**, *29*, 2398−2403.
(24) Ellerby, L. M.; Cabelli, D. E.; Graden, J. A.; Valentine, J. S. *J. Am. Chem. Soc.* **1996**, *118*, 6556−6561.
(25) Shen, J.; Subramaniam, S.; Wong, C. F.; McCammon, J. A. *Biopolymers* **1989**, *28*, 2085−2096.
(26) Falconi, M.; Gallimbeni, R.; Paci, E. *J. Comput. Aided Mol. Des.* **1996**, *10*, 490−498.
(27) Chillemi, G.; Falconi, M.; Amadei, A.; Zimatore, G.; Desideri, A.; Di Nola, A. *Biophys. J.* **1997**, *73*, 1007−1018.
(28) Shen, J.; McCammon, J. A. *Chem. Phys.* **1991**, *158*, 191−198.
(29) Wong, Y.; Clark, T. W.; Shen, J.; McCammon, J. A. *Mol. Simul.* **1993**, *10*, 227−289.
(30) Carloni, P.; Blöchl, P. E.; Parrinello, M. *J. Phys. Chem.* **1995**, *99*, 1338−1348.
(31) Banci, L.; Carloni, P.; Penna, G. L.; Orioli, P. L. *J. Am. Chem. Soc.* **1992**, *114*, 6994−7001.
(32) Banci, L.; Carloni, P.; Orioli, P. L. *Proteins Struct. Funct. Genet.* **1994**, *18*, 216−230.
(33) Mouesca, J.-M.; Chen, J. L.; Noodleman, L.; Bashford, D.; Case, D. A. *J. Am. Chem. Soc.* **1994**, *116*, 11898−11914.

functional theory and electrostatic modeling, based on our recently developed three-region continuum dielectric method which accounts for both protein and solvent environments in the energy calculations.[34] This method has been applied to the study of the redox potentials of FeS proteins like *Anabaena* ferredoxin, phthalate dioxygenase reductase,[34] and MnSOD from *Thermus thermophilus*.[67] In section 2, we describe the model for the CuZnSOD active site and the methods used for quantum and electrostatic calculations. In section 3.1, we present and discuss results of quantum calculations—issues of electronic structure, active-site geometry, and charge distribution. In section 3.2, we discuss energetics of the coupled proton/electron transfer within the solvent/protein extended environment. The main conclusions are summarized in section 4.

2. Methods

We have used our recently developed methods by which the influence of the protein and solvent environments can be incorporated into density functional calculations.[33,34] The method involves treatment of an active-site subset of atoms by detailed quantum mechanical calculations, while the influence of the surroundings is modeled by classical electrostatics. First, density functional (DF) quantum theory calculations are carried out to optimize the geometry and determine the gas-phase energetics of the active-site cluster. Second, a set of atomic point charges for the active-site cluster is fitted according to the electrostatic potential (ESP) of the charge distribution from the DF calculations. Third, the optimized active-site cluster is either docked back into the protein structure or assumed to be surrounded by a uniform dielectric continuum (in the pure solvent calculations). Finally, calculations based on the MEAD (macroscopic electrostatics with atomic detail) model are carried out to find the energetic influence of the solvent or protein/solvent environment. The details of these steps are described in the following subsections.

2.1. Density Functional Calculations. The active site of CuZnSOD was represented with a model consisting of 65 atoms (66 for the protonated structure): 37 heavy atoms and 28 (29) hydrogen atoms, including one water molecule weakly bonded to Cu in the apical position (Figure 1). The starting geometrical coordinates were taken from the experimental X-ray data for the oxidized bovine protein.[35] His44, His46, His69, His78, and His119 were represented by neutral imidazole rings with their β carbon atoms replaced by hydrogen atoms. Asp81 was modeled by an acetate ion. The bridging His61 was represented by imidazolate with its β carbon replaced by a hydrogen atom. The water ligand was initially positioned at a distance of 2.5 Å from the Cu ion. (X-ray structures give a fairly wide range for this Cu(II)−water distance; see Table 1.)

All calculations were carried out using the Amsterdam Density Functional (ADF) package, version 2.3.[36,37] The local density approximation (LDA) for exchange and correlation used the parametrization of Vosko, Wilk, and Nusair (VWN, referred to as V below).[38] To test the accuracy of the model, several corrections (NL) were used: the local correction by Stoll (VS)[39,40] and fully nonlocal (NL) potentials using either Becke's gradient correction to exchange[41] and Perdew's correction to correlation[42,43] (VBP), Becke's gradient correction and the Lee−Yang−Parr correction (BLYP),[44] or the Perdew−Wang corrections to both exchange and correlation (PW91).[45] Convergence was achieved once the maximum element of the commutator of the Fock matrix and density matrix was smaller than 0.0001, using the ADF default parameters. The numerical integration scheme adopted was the polyhedron method developed by te Velde et al.[46] with the accuracy parameter, ACCINT, of 3.5. A set of uncontracted double-ζ Slater-type orbitals (STO) was employed for the main group atoms (H, C, N, O) with single-ζ 3d (carbon, nitrogen, oxygen) or 2p (hydrogen) polarization for all ligand atoms. The Cu and Zn basis sets were triple-ζ with single-ζ 4p polarization. The inner core shells were treated by the frozen core approximation, through Cu(3s, 3p), Zn(3s, 3p), C(1s), N(1s), and O(1s). There were totals of 731 basis functions (Cartesian Slater type functions) used for the nonprotonated model and 736 basis functions used for the protonated structure. A set of auxiliary s, p, d, f, and g STO functions, centered on all nuclei, was introduced to fit the molecular density and to represent Coulomb and exchange potentials accurately. The basis, core, and fit sets correspond to basis set III (H, C, N, O) and basis set IV (Cu, Zn) of ADF 2.3, respectively. All calculations were done with a spin-unrestricted scheme.

Full geometry optimization of cluster models was done according to the analytic gradient method implemented at the LDA level by Versluis et al.[47] and at the NL level by Fan et al.[48] The optimization used the Newton−Raphson method, and the Hessian was updated with the Broyden−Fletcher−Goldfarb−Shanno strategy.[49] Convergence was achieved when changes in coordinate values were less than 0.005 Å and the norm of all gradient vectors was smaller than 0.01.

To model the four possible intermediates in the coupled electron/proton-transfer reaction, the following geometries were fully optimized: the oxidized deprotonated complex (referred to as oxidized, labeled Ox, total charge +2, $S = {}^1/_2$) and reduced deprotonated complex (referred to as reduced nonprotonated, Red$^-$, total charge +1, $S = 0$). Then one proton was added to the bridging histidine Nϵ, and two other

Table 1. Experimental and Calculated (VBP) Geometrical Parameters (Å) for the Oxidized (Ox) and Reduced (Red) Forms of CuZnSOD[a]

Ox	EXAFS[14]	yeast (2.5)[76]	bovine (2.0)[77]	*Xs.*[b] (1.5)[53]	calcd
Cu−His44	1.99	1.86	1.99	1.99	2.07
Cu−His46	1.99	2.22	2.12	2.19	2.07
Cu−His61	1.99	2.17	2.10	2.08	2.04
Cu−His118	1.99	2.16	2.05	2.09	2.06
Cu−water	2.18	2.03	3.00	2.37	2.59
Zn−O(Asp81)	1.96, 2.69			1.99	2.02, 2.48
Zn−C(Asp81)	2.78				2.58
Zn−His61	2.01			2.03	2.07
Zn−His69	2.01			2.05	2.11
Zn−His78	2.01			2.03	2.11

Red	EXAFS[14]	bovine (1.9)[16]	yeast (av) (1.7)[13]	calcd
Cu−His44	1.97	2.15	2.05	1.97
Cu−His46	1.97	2.21	2.11	1.97
Cu−His61		2.17	3.08	3.39
Cu−His118	1.97	2.14	2.10	2.30
Cu−water		2.57	3.15	3.03
Zn−O(Asp81)	1.94, 2.75			2.03, 2.37
Zn−C(Asp81)	2.75			2.54
Zn−His61	2.02			2.09
Zn−His69	2.02			2.12
Zn−His78	2.02			2.12

[a] The resolutions of the various X-ray crystal structures are given in parentheses (in Å). [b] *Xenopus laevis*.

(34) Li, J.; Nelson, M. R.; Peng, C. Y.; Bashford, D.; Noodleman, L. *J. Phys. Chem. A* **1998**, *102*, 6311−6324.
(35) McRee, D. E.; Redford, S. M.; Getzoff, E. D.; Lepock, J. R.; Hallewell, R. A.; Tainer, J. A. *J. Biol. Chem.* **1990**, *265*, 14234.
(36) Baerends, E. J.; Ellis, D. E.; Ros, P. *Chem. Phys.* **1973**, *2*, 41.
(37) Ravenek, W. In *Algorithms and Applications on Vector and Parallel Computers*; te Riele, H. J. J., Dekker, T. J., van de Vorst, H. A., Eds., Elsevier: Amsterdam, 1987.
(38) Vosko, S.; Wilk, L.; Nusair, M. *Can. J. Phys.* **1980**, *58*, 1200−1211.
(39) Stoll, H.; Pavlidou, C. M. E.; Preuss, H. *Theor. Chim. Acta* **1978**, *149*, 143−149.
(40) Stoll, H.; Golka, E.; Preuss, H. *Theor. Chim. Acta* **1980**, *55*, 29−41.
(41) Becke, A. D. *J. Chem. Phys.* **1986**, *84*, 4524−4529.
(42) Perdew, J. P. *Phys. Rev. B* **1986**, *33*, 8822−8824.
(43) Perdew, J. P. *Phys. Rev. B* **1986**, *34*, 7406.
(44) Kohn, W.; Becke, A. D.; Parr, R. G. *J. Phys. Chem.* **1996**, *100*, 12974−12980.
(45) Perdew, J. P.; Chevary, J.; Vosko, S.; Jackson, K. A.; Pederson, M. R.; Singh, D.; Fiolhais, C. *Phys. Rev. B* **1992**, *46*, 6671−6687.
(46) te Velde, G.; Baerends, E. J. *J. Comput. Phys.* **1992**, *99*, 84−98.
(47) Versluis, L.; Ziegler, T. *J. Chem. Phys.* **1988**, *88*, 322−328.
(48) Fan, L.; Ziegler, T. *J. Chem. Phys.* **1991**, *95*, 7401.
(49) Schlegel, B. H. *Adv. Chem. Phys.* **1987**, *67*, 249−285.

Scheme 1

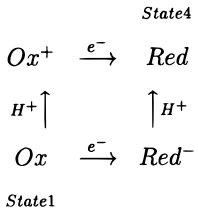

geometries were fully optimized: the oxidized (referred to as oxidized protonated, Ox^+, total charge +3, $S = {}^1/_2$) and reduced (referred to as reduced, Red, total charge +2, $S = 0$) structures. The active-site electronic configurations for all four states are defined as follows: Ox = $Cu^{II}Im^-$, $Ox^+ = Cu^{II}Im$, Red = $Cu^{I}Im$, and $Red^- = Cu^{I}Im^-$, where Im^- = the imidazolate anion and Im = neutral imidazole so that $Im^- + H^+ \rightarrow Im$. The coupled electron/proton reaction is shown in Scheme 1. State 1 is the oxidized nonprotonated form of CuZnSOD, and state 4 is the final reduced protonated complex.

2.2. Fitting of ESP Charges. A modified version of the CHELPG code of Breneman and Wiberg[50] called ChargeFit[51] was used to fit the point charges from the molecular electrostatic potentials (ESP) calculated by the ADF code. The total net charge of the molecule and the three Cartesian dipole moment components from density functional calculations were adopted as constraint conditions for the fit. The fitted points lay on a cubic grid between the van der Waals radius and the outer atomic radius with a grid spacing of 0.1 Å. The outer atomic radius for all atoms used was 5.0 Å, and the van der Waals radii for $Cu^{1,2+}$, Zn^{2+}, C, N, O, and H were 1.5, 1.5, 1.7, 1.55, 1.4, and 1.2 Å, respectively. To minimize the uncertainties in the fitting procedure, the singular-value decomposition (SVD) method[52] was introduced into the code to obtain a model with stable atomic charges and an accurate molecular dipole moment.[33,51]

2.3. Protein Docking. To prepare for calculations of protein/solvent environmental effects, we docked the geometry-optimized active-site model back into the protein. Since there is a quite substantial change in the active-site geometry during the redox process, the two best available geometries from protein X-ray structures were used. (There is an implicit assumption here that the active-site conformational change from the oxidized to the reduced form occurs with the corresponding change in the protein structure oxidized → reduced, and that the latter occurs with no internal protein energy cost via a hinge motion.) The oxidized form of *Xenopus laevis* (Brookhaven Protein Data Bank entry 1XSO, resolution 1.5 Å)[53] was used for the docking of the calculated oxidized cluster, and the reduced form of yeast copper zinc superoxide dismutase (Brookhaven PDB entry 1YSO, resolution 1.7 Å)[13] was used for docking of the reduced nonprotonated and reduced forms of the quantum cluster. A least-squares fitting procedure was performed using two sets of fitting atoms—one set consisted of all heavy atoms of the cluster and the other of a subset of heavy atoms (Cu, Zn, and nitrogen atoms of ligands directly bonded to either Cu or Zn and all heavy atoms of the His61 bridge). The Xfit program, which is part of XtalView package,[54,55] was used for the fitting procedure. Several test redox calculations were conducted with both fitted models, and no significant differences in calculated reduction potentials were found. The model based on a fit of all heavy cluster atoms was used in all subsequent calculations. Protein hydrogen atoms were added at pH 7 using Insight II (MSI) with all heavy atoms fixed. For the discrete water channel models, hydrogen atom positions were similarly added. Minor adjustments were made to give a hydrogen-bonded water network extending from the active site, starting at the bound quantum water molecule.

2.4. Electrostatic Calculations of Protein and Solvent Effects. The effects of the solvent or protein/solvent environment were treated by models of the MEAD (macroscopic electrostatics with atomic detail) type. For an active-site cluster immersed in a pure solvent (without the rest of the protein), the cluster was modeled as a vacuum region (dielectric constant, $\epsilon = 1$) containing the ESP-fit charges and surrounded by a continuum with a dielectric constant equal to that of the bulk solvent. For an active-site cluster docked into a protein, the cluster was again modeled as a vacuum region with ESP-fit charges; the protein was modeled as a region of dielectric constant, ϵ_p, with embedded charges corresponding to the partial charges of the protein atoms, and the solvent region (any space not included in the active-site or protein regions) was modeled as a region of dielectric constant, ϵ_s (usually taken as 80, for water). In the definition of the dielectric regions, the "interior" corresponding to a group of atoms is defined as the region inaccessible to any part of a probe sphere of radius 1.4 Å rolling on radii of the atomic spheres. The boundary beween the interior and exterior so defined is equivalent to Connolly's definition of the molecular surface.[56]. For the pure-solvent case, the vacuum region is the interior of the set of cluster atoms and the exterior is the solvent region. For the protein-docked case, the vacuum region is again the interior of the cluster atoms, the ϵ_p (protein) region is the interior of the protein atom set, exclusive of any volume lying within the cluster interior, and all remaining volume is the ϵ_s (solvent) region. For the protein dielectric constant, we have generally used the value $\epsilon_p = 4$ (see section 3.2).

In the pure-solvent case, the solvation free energy of the cluster is ${}^1/_2 \sum_i q_i \phi_{react}(x_i)$, where the q_i are the cluster charges located at the points x_i and ϕ_{react} is the reaction potential of these charges, that is, the potential produced by the response of the surrounding dielectric media to these charges. The factor ${}^1/_2$ takes into account the work needed to polarize the dielectric media within linear response theory. This is a straightforward generalization of the classical Born theory of ion solvation.[57]

In the case of the active-site cluster docked into a protein, the total electrostatic interaction energy of the active-site quantum cluster with the protein/solvent environment is the sum of two terms:[34] the reaction-field term, E_r, and the protein-field term, E_p. The reaction-field term is very similar to that in the pure-solvent case, except that ϕ_{react} now arises from the protein and solvent dielectric regions. The protein-field term (which roughly corresponds to the "background" term in protein titration calculations[58]) arises from the interaction of the cluster with the potential produced by the protein atomic partial charges. For the second term, the protein-field potential, ϕ_{prot}, is generated by the protein atomic partial charges; that is, $E_p = \sum_i q_i \phi_{prot}(x_i)$. The protein-field potential incorporates screening by the protein and solvent dielectric media. One significant point for later analysis is that the protein interaction energy (and the protein potential, ϕ_{prot}) is linear in the contributions from the different protein atomic charges and, therefore, from the different protein residues (or the main-chain/side-chain parts of these). The sum of the reaction-field and protein-field terms is designated $E_{pr} \equiv E_r + E_p$ and is taken as the free energy of transferring the active-site cluster into the protein/solvent environment.

The reaction potential, ϕ_{react}, is the difference between the solution of the Poisson equation for the potential due to the active-site cluster charges in the dielectric environment of interest and the potential due to these same charges in a vacuum. The protein potential, ϕ_{prot}, is the solution of the Poisson equation for the potential due to the protein's charges in the three-dielectric environment of vacuum, protein, and solvent. The relevant Poisson equations were solved using the finite-difference method[52] with a series of successively finer cubic lattices centering around the active site. For the pure-solvent cases, the numbers of lattice points were 91^3 101^3, and 107^3 with linear spacings of 1.0, 0.25, and 0.15 Å, respectively. For the protein-docked cases, the numbers of lattice points were 131^3, 131^3, and 131^3 with linear spacings

(50) Breneman, C. M.; Wiberg, K. B. *Comput. Chem.* **1990**, *11*, 361−373.
(51) Chen, J. L.; Noodleman, L.; Case, D. A.; Bashford, D. *J. Phys. Chem.* **1994**, *98*, 11898−11914.
(52) Press, W. H.; Flannery, B. P.; Teukolsky, S. A.; Vetterling, W. T. *Numerical Recipes. The Art of Scientific Computing*; Cambridge University Press: Cambridge, England, 1986.
(53) Djinović Carugo, K.; Battistoni, A.; Carri, M. T.; Polticelli, F.; Desideri, A.; Rotilio, G.; Coda, A.; Wilson, K. S.; Bolognesi, M. *Acta Crystallogr.* **1996**, *D52*, 176−188.
(54) McRee, D. E. *J. Mol. Graphics* **1992**, *10*, 44−46.
(55) McRee, D.; Israel, M. In *Crystallographic Computing 7*; Bourne, E., Watenpaugh, K., Eds.; Oxford University Press: Oxford, England, 1998.
(56) Connolly, M. L. *Science* **1983**, *221*, 709.
(57) Born, M. *Z. Phys.* **1920**, *1*, 45−48.
(58) Bashford, D.; Gerwert, K. *J. Mol. Biol.* **1992**, *224*, 473−486.

Scheme 2

$$\begin{array}{ccccccc} (g) & Red^- & \longrightarrow & Ox & + & e^- \\ & \downarrow & & \downarrow & & \downarrow \\ (s) & Red^- & \longrightarrow & Ox & + & e^- \end{array}$$

Scheme 3

$$\begin{array}{ccccccc} (g) & Red & \longrightarrow & Red^- & + & H^+ \\ & \downarrow & & \downarrow & & \downarrow \\ (s) & Red & \longrightarrow & Red^- & + & H^+ \end{array}$$

of 1.0, 0.25, and 0.15 Å, respectively. The active-site atomic radii used to define the dielectric boundary were 1.5 ($Cu^{+,2+}$, Zn^{2+}), 1.7 (C), 1.55 (N), 1.4 (O), and 1.2 Å (H), which is consistent with our past experience in both organic systems and transition metal complexes.[51,59,60] The protein atom partial charges and radii (for defining the protein dielectric region) were taken from the widely used PARSE charge set of Sitkoff, Sharp, and Honig.[61] The electrostatic calculations were done using the MEAD program suite developed previously.[58,62] (The MEAD computer programs are available through the Internet by anonymous FTP to ftp.scripps.edu under the directory "electrostatics" or through the Bashford Web page, http://www.scripps.edu/bashford.)

The methodology of pK_a and reduction potential calculation has been described elsewhere.[51,63] Here we summarize the necessary steps for calculating the pK_a and redox potential for coupled electron/proton transfer in a solution. The coupled electron/proton reaction in aqueous solution (state 1 → state 4, Scheme 1) can be formally separated into two steps: the electron transfer (energetics shown in Scheme 2) and the protonation step with corresponding energetics shown in Scheme 3. In Schemes 2 and 3, (g) and (s) represent gas and solvent phase, respectively. In this description, the terms "solvent phase" and "solvation" can be understood to refer either to a pure-solvent environment or, in the case of the protein-docked calculations, to the protein/solvent environment.

The energy required for the electron transfer (E_{ET}) can be expressed as

$$E_{ET} = IP_{(g)} + \Delta E_{PB} + \Delta SHE \quad (1)$$

The $IP_{(g)}$ is defined as the gas-phase ionization potential on going from the reduced nonprotonated to the oxidized state ($IP_{(g)} = E_{(g)}(Ox) - E_{(g)}(Red^-)$), ΔE_{PB} is the difference in solvation energies for oxidized minus reduced nonprotonated systems, and ΔSHE is the standard hydrogen electrode potential correction of −4.43 eV,[64] corresponding to the $\Delta G_{(s)}(H^+)$ value of −260.5 kcal/mol.

The energy of proton transfer (negative of the protonation free energy, $-E_{PT}$) is calculated from the pK_a of the reduced form (Red):

$$1.37pK_a = PA_{(g)}(Red) - T\Delta S_{(g)}(H^+) - \Delta G_{(s)}(Red) + \Delta G_{(s)}(Red^-) + \Delta G_{(s)}(H^+) \quad (2)$$

$$PA_{(g)} = E_{deprot} + \Delta ZPE + {}^5/_2RT \quad (3)$$

$$-E_{PT} = (pK_a - 7)1.37/23.06 \quad (4)$$

where $PA_{(g)}$ is the system's gas-phase proton affinity, E_{deprot} is the deprotonation energy, and ΔZPE is the zero point energy difference of the deprotonated minus the protonated state. Since the calculation of the ΔZPE for the CuZnSOD complex is computationally difficult, the ΔZPE value of −8.4 kcal/mol was taken from vibrational frequency calculations for the histidine molecule (H_{vib}(His) − H_{vib}(His−H)). $\Delta G_{(s)}$(Red), $\Delta G_{(s)}(Red^-)$, and $\Delta G_{(s)}(H^+)$ are solvation free energies of the reduced and reduced nonprotonated complexes and the proton, respectively. Also, $-T\Delta S_{(g)}(H^+)$ is the free energy associated with the gas-phase translational entropy of a proton, estimated as 34 eu or −7.2 kcal/mol at 298 K.

The total redox potential is then the sum of the electron-transfer energy and the negative of the protonation free energy:

$$E^\circ_{redox} = -E_{PT} + E_{ET} \quad (5)$$

The pK_a of the oxidized protonated form (Ox^+) can be calculated by modifying eqs 2 and 3:

$$1.37pK_a = PA_{(g)}(Ox) - T\Delta S_{(g)}(H^+) - \Delta G_{(s)}(Ox^+) + \Delta G_{(s)}(Ox) + \Delta G_{(s)}(H^+) \quad (6)$$

$$PA_{(g)} = E_{deprot} + \Delta ZPE + {}^5/_2RT \quad (7)$$

where $\Delta G_{(s)}(Ox^+)$, $\Delta G_{(s)}(Ox)$, and $\Delta G_{(s)}(H^+)$ are solvation energies of the oxidized protonated and oxidized forms and the proton, respectively.

3. Results and Discussion

3.1. Quantum Calculations. 3.1.1. Geometry Optimized Structures. The active-site model was geometry optimized completely (over all degrees of freedom) in oxidized, oxidized protonated, reduced, and reduced nonprotonated forms. Several nonlocal functionals (VBP, BLYP, PW91) and also a local functional (VS) were used. In addition, after full VS optimization, we used the simpler VBP single-point energy evaluation (called VS/VBP). The calculations which employed the local VS approximation yield greater metal−ligand bond strengths and give shorter metal−ligand distances than the nonlocal functionals (see Supporting Information, Tables S1−S4), as expected for this level of theory.[65] As seen previously, VS and nonlocal potentials (BLYP, VBP, PW91) largely bracket the expected bond length range. All nonlocal approximations gave very similar results for geometries and are in very good agreement with the experiment. (The corresponding energies are analyzed later.) Comparison of selected calculated (VBP) and experimental geometrical parameters for the oxidized and reduced states is shown in Table 1. The VBP optimized structures for the oxidized and reduced forms are shown in Figures 2 and 3, respectively. Selected calculated geometrical parameters (at the full nonlocal VBP level) for the reduced nonprotonated and oxidized protonated forms are presented in Table 2.

The rms deviations in Cu−ligand and Zn−ligand bond distances comparing our VBP calculations with the highest resolution X-ray structures are 0.09 Å for the oxidized structure (*Xenopus laevis*, *Xs*. structure)[53] and 0.19 Å for the reduced structure (yeast structure).[13] These rms deviations are within expected experimental bond length uncertainties. The most significant difference between the predicted and experimental bond length parameters is in the Cu−O(water) bond distance. This discrepancy can be attributed largely to the experimental uncertainty in the position of the Cu-bound water molecule

(59) Bondi, A. *J. Chem. Phys.* **1964**, *64*, 441.
(60) Li, J.; Fisher, C. L.; Chen, J. L.; Bashford, D.; Noodleman, L. *Inorg. Chem.* **1996**, *35*, 4694−4702.
(61) Sitkoff, D.; Sharp, K. A.; Honig, B. *J. Phys. Chem.* **1994**, *98*, 1978.
(62) Bashford, D. An object-oriented programming suite for electrostatic effects in biological molecules. In *Scientific Computing in Object-Oriented Parallel Environments*; Ishikawa, Y., Oldehoeft, R. R., Reynders, J. V. W., Tholburn, M., Eds.; Lecture Notes in Computer Science, Vol. 1343; Springer: Berlin, 1997; pp 233−240.
(63) Fisher, C. L.; Chen, J.-L.; Li, J.; Bashford, D.; Noodleman, L. *J. Phys. Chem.* **1996**, *100*, 13498−13505.
(64) Reiss, H.; Heller, A. *J. Phys. Chem.* **1985**, *89*, 4207−4213.
(65) Li, J.; Noodleman, L. In *Spectroscopic Methods in Bioinorganic chemistry*; Solomon, E. I., Hodgeson, K. O., Eds.; ACS Symposium Series 692; American Chemical Society: Washington, DC, 1998.

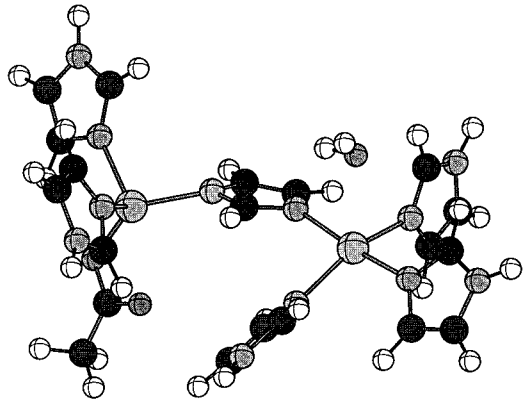

Figure 2. VBP optimized geometry of the oxidized active site in CuZnSOD.

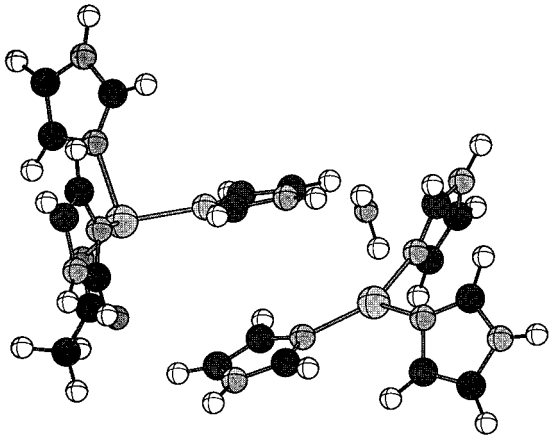

Figure 3. VBP optimized geometry of the reduced active site in CuZnSOD.

Table 2. Calculated (VBP) Geometrical Parameters for the Reduced Nonprotonated (Red^-) and Oxidized Protonated (Ox^+) Forms of CuZnSOD and Those for a Second Higher Local Minimum Geometry Found for the Reduced Form Compared with the Reduced (Red) and Oxidized (Ox) Calculated Geometries (Å)

	Red	Red^-	Red^- (2nd local min)	Ox^+	Ox
Cu−His44	1.97	2.01	2.03	2.00	2.07
Cu−His46	1.97	1.98	2.00	1.98	2.07
Cu−His61	3.39	2.95	2.64	3.46	2.04
Cu−His118	2.30	2.18	2.21	2.07	2.06
Cu−water	3.03	3.09	3.08	3.09	2.59
Zn−O(Asp81)	2.03, 2.37	2.04, 2.42	2.05, 2.39	2.06, 2.50	2.02, 2.48
Zn−C(Asp81)	2.54	2.56	2.55	2.67	2.58
Zn−His61	2.09	2.01	2.02	2.09	2.07
Zn−His69	2.12	2.12	2.13	2.08	2.11
Zn−His78	2.12	2.15	2.17	2.10	2.11

(which is weakly coordinated) in the narrow active-site channel, as is seen from the variability in the Cu−O(water) distance among the different X-ray structures and EXAFS. The calculated Cu−water distance lies within the interval spanned by the experimental structures.

We also note that there is a tendency of the Asp81 ligand to bind in a pseudobidentate fashion to the Zn metal site in our model. Since we have performed a full optimization of the molecule, there is more conformational freedom in our model than in the enzyme, where a hydrogen bond between Asp81 and Gly70 restrains movement of the Asp81. The calculated bond distance between Zn and the second oxygen in Asp81 is on average shorter by 0.2 Å for the oxidized and by 0.4 Å for the reduced state, respectively, than the corresponding experimental distances from EXAFS. Since this structural distortion will not significantly change the charge distribution on the Zn/Cu centers, we expect that its effect on calculations of overall energetics and reduction potentials is fairly minor.

The His61 Nϵ−Cu bond is elongated (from 2.04 Å in Ox to 2.95 Å in Red^-) during the reduction and finally stretched to 3.39 Å upon protonation. At such a long distance, the His61 Nϵ−Cu bond is broken (Figure 3). The elongation and breaking of the His61 Nϵ−Cu bond may be attributed to several factors. However, it can be explained in part by the molecular orbital analysis. Since the interaction of the oxidized CuZnSOD and superoxide is a one-electron reduction, the lowest unoccupied molecular orbital (LUMO) plays an important role in this process. Figure 4 shows the LUMO of the oxidized structure and the HOMO of the reduced protonated structure. The major contributions to the LUMO of the oxidized structure are from d orbitals of Cu and p orbitals of N atoms bonded to the Cu ion (Table 3 and Figure 4). Upon addition of one electron to the LUMO during the reduction, the principal interaction becomes the antibonding interaction among the Cu d_{z^2}, $d_{x^2-y^2}$ and His61 Nϵ p_z orbitals. This leads to the longer His61 Nϵ−Cu bond. During the elongation, the His61 ring tilts away from the copper ion and, simultaneously, the position of the Cu ion shifts relative to His61. This results in an increase in the Cu−His61 distance from 2.04 Å in the oxidized form to 2.95 Å in reduced nonprotonated form (Red^-) and to 3.39 Å in the reduced protonated form (Red), respectively. During the optimization of the reduced nonprotonated form, we have found a second, higher-energy local minimum which corresponds to a geometry with a His61 Nϵ−Cu bond distance of 2.64 Å. All other bond lengths and angles are similar to those in the fully optimized reduced nonprotonated form. This complex in the gas phase is 2.2 kcal/mol higher in energy than the reduced nonprotonated geometry with a His61 Nϵ−Cu bond length of 2.95 Å. This suggests that the potential energy surface associated with the process of the His61 Nϵ−Cu bond elongation upon reduction is fairly flat.

The calculated energy minimum geometry for the reduced form is a structure with the His61 Nϵ−Cu bond broken. This predicted geometry is consistent with most of the X-ray experiments.[13,14] However, a reduced enzyme structure with the His61 Nϵ−Cu bond intact was also reported.[15,16] One possible explanation for this result is that redox heterogeneity may exist in some crystal preparations used in obtaining X-ray structures of CuZnSOD, so that, in these cases, the observed geometry is a mixture of the two oxidation state structures. Similar problems of redox heterogeneity were reported recently for the MnSOD resting state, which may be in a mixture of oxidation states, on the basis of EPR spectra seen for preparations similar to those used for X-ray structures.[66] Our calculations also indicate that redox heterogeneity is quite probable for MnSOD, on the basis of calculated geometries versus experimental X-ray structures.[67]

During reduction and protonation, the His61 ring tilts slightly away from the Cu ion, forming a hydrogen bond between the His61 Nϵ−H hydrogen atom and the water molecule. There are other possible geometries with different orientations of the water molecule with respect to the active site but they all should be energetically very similar. There are no significant changes in the Zn site geometry during the reduction and protonation.

3.1.2. Energetics and Charge Distribution. The one-electron

(66) Whittaker, J. W.; Whittaker, M. M. *J. Am. Chem. Soc.* **1991**, *113*, 5528.
(67) Li, J.; Fisher, C. L.; Konecny, R.; Bashford, D.; Noodleman, L. *Inorg. Chem.* **1999**, *38*, 929.

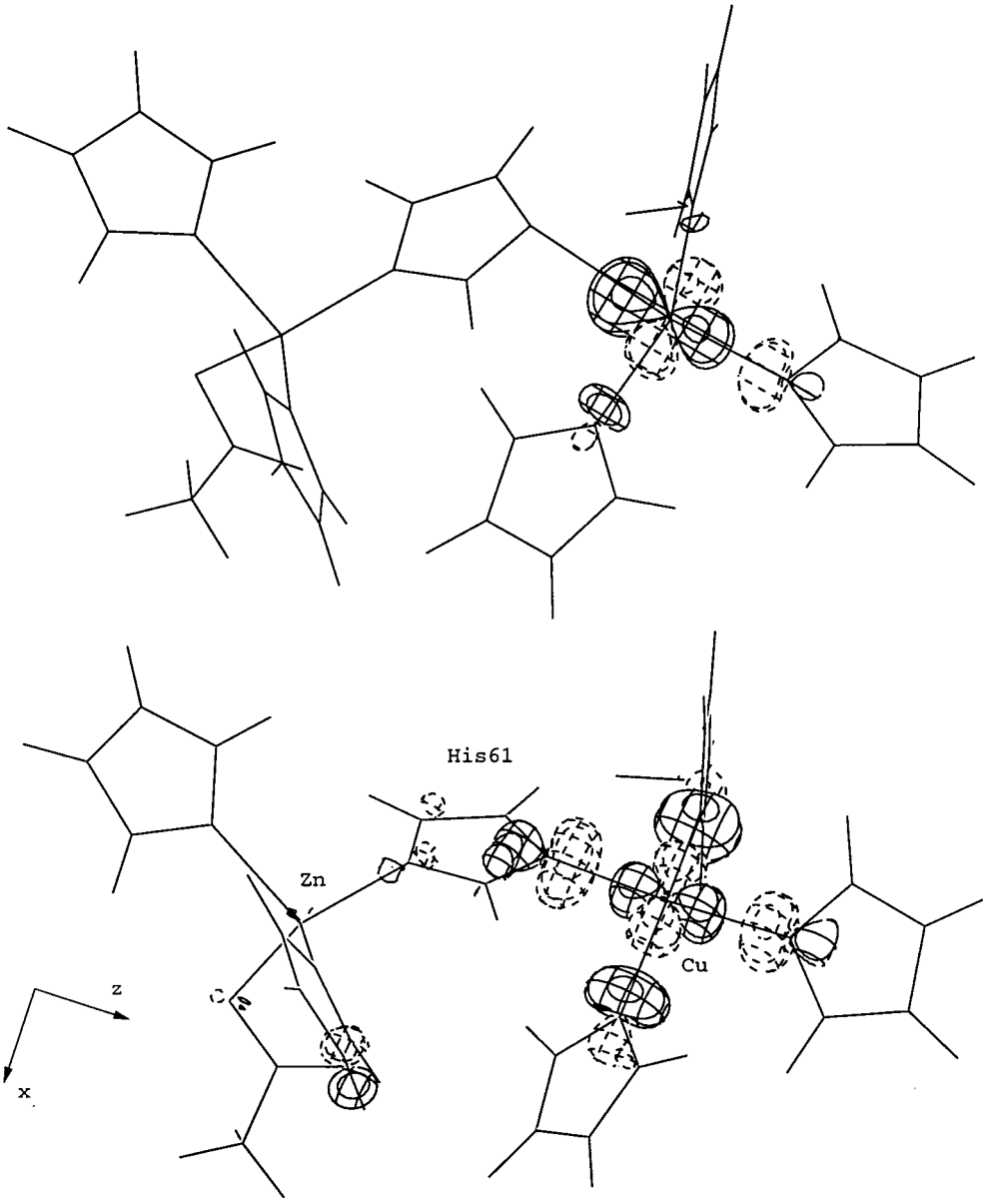

Figure 4. LUMO (bottom) of the CuZnSOD oxidized form and HOMO (top) of CuZnSOD reduced protonated form. The *x* and *z* axes of the coordination system are shown; Cu is in the center of the coordination system. The figure was prepared using program viewkel, part of the YAeHMOP program suite.[78]

Table 3. LUMO Populations of the CuZnSOD Oxidized Structure (%)[a]

	AO contribn to the LUMO		AO contribn to the LUMO
Cu d_{z^2}	38.0	His44 Nδ p_x	5.4
His61 Nϵ p_z	7.9	His118 Nϵ p_z	4.7
Cu $d_{x^2-y^2}$	6.4	His46 Nϵ p_x	3.8

[a] Only contributions larger than 3% are shown.

reduction of the copper zinc superoxide dismutase ($Ox + e^- \rightarrow Red^-$) is energetically favored by 8.25 eV (at the VBP level) (adiabatic electron affinity of Ox in the gas phase) and the following proton transfer ($Red^- + H^+ \rightarrow Red$) (adiabatic proton affinity of Red^- in the gas phase) by 9.09 eV. The total energy change for the coupled proton- and electron-transfer reduction of CuZnSOD is −17.34 eV as calculated at the VBP level in the gas phase (that is, without considering the protein/solvent interaction energy).

The VBP ESP calculated charge distribution on the metals in the complex and atoms bonded to them is shown in Table 4. The charge on the zinc ion is larger than that on the copper ion, in contrast with the earlier theoretical prediction.[68] As can be observed from Table 4, there is a significant delocalization of the incoming electron during the reduction ($Ox + e^- \rightarrow Red^-$) due to electron relaxation. This maintains a significant positive charge on the copper ion so it can still attract a subsequent (second) superoxide anion in the catalytic cycle.

Table 5 shows the VBP calculated gas-phase ESP charges per residue for the oxidized, reduced nonprotonated, reduced, and oxidized protonated forms of CuZnSOD. During the first step of the reaction ($Ox + e^- \rightarrow Red^-$), the incoming electron is delocalized on His ligands bonded to the copper ion (His44, His46, His61, and His118) and also on the zinc ion. After the proton-transfer step ($Red^- + H^+ \rightarrow Red$), the total charge on the His61 ligand changes from −0.325 to +0.154 mainly due to the transferred proton. There is also a net increase of the positive charge on the Cu ion and surrounding His and water

(68) Shen, J.; Wong, C. F.; Subramaniam, S.; Albright, T. A.; McCammon, J. A. *J. Comput. Chem.* **1990**, *11*, 346−350.

Table 4. VBP Calculated Gas-Phase ESP Charges of Selected Atoms for the Oxidized (Ox), Reduced Nonprotonated (Red^-), Reduced (Red), and Oxidized Protonated (Ox^+) Geometries

	Ox	Red^-	Red	Ox^+
tot. charge	+2	+1	+2	+3
Cu	0.445	0.444	0.385	0.582
His44 Nδ	−0.116	−0.147	−0.191	−0.189
His118 Nϵ	−0.156	−0.250	−0.082	−0.178
His46 Nϵ	0.025	−0.160	−0.170	−0.209
His61 Nϵ	0.117	−0.094	−0.104	−0.114
Zn	0.801	0.682	0.721	0.737
His69 Nδ	−0.218	−0.155	−0.147	−0.154
His61 Nδ	−0.356	−0.127	−0.180	−0.204
His78 Nδ	−0.140	−0.124	−0.164	−0.181
Asp81 O	−0.455	−0.439	−0.442	−0.366
Asp81 O	−0.384	−0.412	−0.467	−0.380
Wat O	−0.571	−0.563	−0.574	−0.613
Wat H	0.346	0.274	0.347	0.386
Wat H	0.197	0.147	0.211	0.270
His61 H			0.258	0.261

Table 5. VBP Calculated Gas-Phase ESP Charges per Residue for the Oxidized (Ox), Reduced Nonprotonated (Red^-), Reduced (Red), and Oxidized Protonated (Ox^+) Geometries

	Ox	Red^-	Red	Ox^+
tot. charge	+2	+1	+2	+3
Cu	0.445	0.444	0.385	0.582
His44	0.286	0.144	0.199	0.285
His118	0.294	0.090	0.252	0.325
His46	0.341	0.153	0.256	0.340
His61	−0.184	−0.325	0.154	0.176
Zn	0.801	0.682	0.721	0.737
His69	0.208	0.203	0.247	0.302
His78	0.287	0.232	0.261	0.417
Asp81	−0.453	−0.481	−0.461	−0.205
Wat	−0.028	−0.142	−0.016	0.043

ligands (total). The zinc positive charge also increases with protonation of the bridge. The subsequent removal of an electron ($Red \rightarrow Ox^+ + e^-$) raises the positive charge on all residues included in our model. This ESP charge change during the electron/proton coupled transfer reaction suggests that there is a very efficient mechanism of charge delocalization in CuZn-SOD. This mechanism mainly involves the Cu ion and surrounding histidine and water ligands, but the Zn ion is also actively involved in this process.

Our calculated energies suggest that, even in the gas phase, the Ox^+ form is not favored, and the reaction proceeds from the reduced form (Red) to the reduced nonprotonated form (Red^-) and then to Ox, rather than first to the oxidized protonated complex (Ox^+) and then to the oxidized nonprotonated state (Ox). This is also supported by the reaction energy calculation which predicts that in the gas phase the $Red \rightarrow Ox^+ + e^-$ step requires an energy of +11.74 eV compared to the $Red \rightarrow Red^- + H^+$ step, which requires only +9.09 eV (at the VBP level). Overall, it is likely that the reduction and protonation of the second superoxide to the hydroperoxide anion occurs in a highly coupled (concerted) reaction: $O_2^- + e^- + H^+ \rightarrow (HO_2)^-$. The acidity of Ox^+ in a complete protein/solvent environment will be analyzed later.

3.2. Effect of the Solvent and Protein Environment. For calculations pertaining to the active-site model immersed in water, but without the protein environment, the selection of the appropriate MEAD model for the solvation energy terms is straightforward.[60,63,69] The solvent region is assigned the bulk dielectric constant of water, while the quantum region is assigned $\epsilon = 1$ (see section 2.4). Introduction of the protein environment into calculations for the electron- and proton-transfer processes raises complex issues concerning the protein's response to these processes. In the present calculations, we have made use of distinct X-ray crystallographic structures for the oxidized and reduced states, so that the protein's conformational change in response to electron transfer is modeled explicitly. However, there are no X-ray crystallographic structures available for both states of the proton-transfer process of interest, Red ↔ Red^-; instead, the available structure corresponds to the protonated form, Red, alone. In situations of the latter kind, it has been common to model the response of the protein implicitly through the choice of a protein dielectric constant that accounts for some conformational response, as well as an electronic response, to charge-altering processes;[70,71] and in the present work, we have chosen the value $\epsilon = 4$, which is consistent with many experimental and theoretical studies, at least for the protein interior.[72−74] It could be argued that this choice is problematic with respect to the electron-transfer parts of the calculations, since the response of the protein is being counted twice, once through the explicit changes from the Ox to Red protein structure and again through the protein dielectric constant. It might seem preferable to use $\epsilon = 2$, a value that would account only for the electronic polarizability of the protein. However, the redox process in which we are most interested is the coupled electron and proton transfer, Ox ↔ Red, which is an overall electroneutral process. As will be shown presently, this process is fairly insensitive to the choice of dielectric constant. On the other hand, the proton-transfer process of interest, Red ↔ Red^-, is not electroneutral and is quite sensitive to the dielectric constant. Therefore, our choice of dielectric constant is driven more by consideration of the proton-transfer process, for which $\epsilon = 4$ is probably the most appropriate choice.

Table 6. CuZnSOD pK_a[a] and Redox Potential[b] Values in (A) the Continuum Dielectric ($\epsilon = 80.0$), (B) the Protein Represented by One Subunit with Continuum Water, (C) One Subunit with Eight Discrete Water Molecules in the Active Channel, (C′) Extended Model C (See Text), (D) the Dimer with All X-ray Water Molecules, and (D′) Extended Model D

	A	B	C	C′	D	D′	expt
pK_a	9.43	8.21	10.62	11.68	11.45	12.47	10.7[23]
E°_{redox} (V)	0.582	0.698	0.853	0.890	0.412	0.434	0.403[21]

[a] pK_a value of the His61 Hϵ proton in reduced protonated structure Red. [b] Coupled redox potential for $Ox + H^+ + e \rightarrow Red$.

In Table 6, we present our calculated redox potentials for a number of different models, reflecting the coupled one-electron transfer plus proton transfer (at pH = 7). The calculated pK_a for the protonated imidazole (His61) of the reduced Cu(I) complex is also reported. All these calculations used the VBP potential and full geometry optimization for the isolated cluster. All of the models contained the active-site quantum cluster defined above. In model A, the quantum cluster is placed in the solvent continuum dielectric alone. The other models include the remainder of the protein as a medium with a dielectric constant of 4 but differ in the representation of the waters in the channel near the Cu active site, in some waters on the protein surface, and in whether a (C) monomer protein subunit or (D)

(69) Mouesca, J.-M.; Chen, J. L.; Noodleman, L.; Bashford, D.; Case, D. A. *J. Am. Chem. Soc.* **1994**, *116*, 11898−11914.
(70) Honig, B.; Nicholls, A. *Science* **1995**, *268*, 1144−1149.
(71) Yang, A.-S.; Gunner, M. R.; Sampogna, R.; Sharp, K.; Honig, B. *Proteins* **1993**, *15*, 252−265.
(72) Bone, S.; Pethig, R. *J. Mol. Biol.* **1985**, *181*, 323.
(73) Simonson, T.; Perahia, D. *Proc. Natl. Acad Sci U.S.A.* **1995**, *92*, 1082−1086.
(74) Simonson, T.; Perahia, D. *J. Am. Chem. Soc.* **1995**, *117*, 7987−8000.

Table 7. Electrostatic Interaction Energy Components (kcal/mol) (VBP) for the Oxidized and Reduced Protein in Different Environments[a]

	B	C	D
Ox			
reaction field	−125.58	−121.70	−118.28
protein field	−17.05	−21.12	−38.88
tot. electrostat energy	−142.63	−142.82	−157.46
Red			
reaction field	−128.49	−126.28	−123.35
protein field	−14.53	−22.77	−28.39
tot. electrostat energy	−143.20	−149.05	−153.53

[a] Models: (B) protein represented by one subunit with continuum water; (C) one subunit with eight discrete water molecules in the active channel; (D) dimer with all X-ray water molecules.

dimer was used. In model B, all waters are treated by the continuum method (other than the active-site water bonded to Cu, which is part of the quantum active site for all models). For model C, the eight closest water molecules (other than the single quantum water) found from X-ray crystallography in the active-site cavity were treated as discrete water molecules (partial charge model for H_2O from an ESP fit for an H_2O molecule in a vacuum, and dielectric constant $\epsilon = 4$, as used for the protein). For model D, all water molecules found from X-ray crystallography are treated as discrete; these fill the active channel and include some protein surface waters as well. The remaining water volume is treated as continuum bulk water ($\epsilon = 80$) for models C and D. Models C and D represent the possibility that the specific structure of the water near the active site, and the manner in which that structure changes in the redox process, affects the active-site energetics in a way that cannot be adequately represented by the bulk dielectric response. Compared to the experimental redox potential +0.40 V,[21] the calculated redox potentials in the full protein environment agree best when all X-ray waters are included (model D, $E^\circ_{redox} = +0.41$ V), but model C, with eight additional discrete water molecules, agrees less well with the experimental redox potential than model B, with only the "quantum" water. The behavior of the purely continuum water model A ($\epsilon = 80$) is surprisingly good ($E^\circ_{redox} = +0.58$ V) and indicates that the protein beyond the active site acts much as a stabilizing aqueous medium. The inclusion of the second subunit in the dimer does not have a significant effect on the result. The predicted reduced complex imidazole pK_a's for models A, C, and D are also in reasonable agreement with the experimental pK_a of 10.8, while model B shows a larger discrepancy with experiment.

Table 7 shows the total electrostatic interaction energy components for the CuZnSOD within the extended environment with the VBP exchange-correlation potential for the quantum cluster. The greatest stabilization comes from the dielectric−cluster interaction (reaction field) component of the total electrostatic energy. The protein field−cluster interaction is also stabilizing but smaller. The net effect of going to more discrete water molecules in the model is that the magnitude of the protein-field interaction energy increases while the magnitude of the reaction-field contribution decreases.[75−78]

We have also used the simple model A to test the quality of different exchange-correlation potentials for accurately predicting redox potentials and pK_a's. Table 8 shows that while all exchange-correlation potentials tested give very good quality geometries (see Supporting Information), the purely local VS potential is very poor for redox energies and so is the nonlocal BLYP method. In contrast, the mixed VS/VBP method gives redox potentials and pK_a's in very good agreement with the fully nonlocal VBP and PW91 methods. These three methods are then suitable for calculating both optimized geometries and energies.

Table 8. CuZnSOD pK_a and Redox Potential Values for Different Functionals Calculated by Using Model A, the Continuum Solvent Model[a]

	VS	BLYP	VBP	VS/VBP	PW91	expt
pK_a	6.64	13.22	9.43	11.46	10.10	10.7[23]
E°_{redox} (V)	−0.382	1.923	0.582	0.529	0.561	0.403[21]

[a] See text.

Table 9. pK_a and Redox Potential Values for CuZnSOD Calculated at the VBP Level for Different Values of Solvent Dielectric Constant (ϵ) with the Continuum Solvent Model

	ϵ		
	80.0	4.0	1.0
pK_a	9.43	−3.88	−47.5
E°_{redox} (V)	0.582	0.573	0.585

Table 9 shows results of a study of pK_a and the redox potential dependence on the solvent dielectric constant. We have performed calculations of pK_a and E°_{redox} for the quantum cluster (VBP) immersed in an aqueous solvent ($\epsilon = 80$) and in a solvent with a dielectric constant corresponding to the pure protein environment ($\epsilon = 4$) and with $\epsilon = 1$, which essentially turns the solvent interactions off. As expected for an electroneutral reaction, the redox potential does not depend greatly on the dielectric constant. However, inclusion of high dielectric solvation is necessary for the correct calculation of pK_a.

To arrive at the energetics of the oxidized protonated complex (Ox^+) in a solvent, the pK_a of the deprotonation step ($Ox^+ \rightarrow Ox + H^+$) was calculated. The p$K_a$ of Ox^+ in aqueous solution (without the full protein environment, corresponding to model A) is −9.18. This extreme acidity confirms that Ox^+ has very high energy and would release the His61 Nϵ bound proton and convert to the Ox form. This energetic preference for the Ox form in a solvent environment agrees with the predictions from the gas-phase calculation and also should apply in the protein/solvent environment.

To study the influence of the histidine bridge and the Zn ion on the acidity of the His61 Nϵ−H proton, we calculated the pK_a of the Zn−His61 fragment, i.e. the fragment which includes bridging His61, Zn^{2+}, Asp81, His69, and His78. The pK_a for the His61 Hϵ proton of this fragment in a continuum dielectric (aqueous solution only, corresponding to model A) is +11.5, which is moderately less acidic than the full CuZnSOD complex (pK_a = 9.43 in pure solvent, Table 8). This suggests that the zinc site in the CuZnSOD is responsible for most of the basicity of the CuZnSOD. The addition of the positively charged Cu ion in the full CuZnSOD complex makes the His61 Nϵ−H proton more acidic, which increases its availability for the reaction. Further, the protein/solvent models with discrete water (C and D) yield more basic pK_a values than the continuum water model (A). The protein residue making the largest contribution to this upward pK_a shift was found to be Asp122, which bridges His44 and His69, which are coordinated to the metals (Figure 5). Asp122 shifts the pK_a more basic by ΔpK_a = 4.6 units (model D) on the basis of its contributions to the protein-field

(75) Chan, S. L.; Lim, C. *J. Phys. Chem.* **1994**, *98*, 692−695.
(76) Djinović, K.; Gatti, G.; Coda, A.; Antolini, L.; Pelosi, G.; Desideri, A.; Falconi, M.; Marmocchi, F.; Rotilio, G.; Bolognesi, M. *J. Mol. Biol.* **1992**, *225*, 791−809.
(77) Tainer, J. A.; Getzoff, E. D.; Beem, K. M.; Richardson, J. S.; Richardson, D. C. *J. Mol. Biol.* **1982**, *160*, 181−217.
(78) Landrum, G. A. *Yet Another Extended Hückel Molecular Orbital Package (YAcHMOP)*; Cornell University: Ithaca, NY, 1997.

Table 10. Electrostatic Interaction Energy Components (kcal/mol) for the Oxidized, Reduced Nonprotonated, and Reduced Protein in Models C, C′, D, and D′, Along with the Asp122 Residue Contribution[a]

	Ox	Ox_{Asp}	Red^-	Red^-_{Asp}	Red	Red_{Asp}
models C and C′						
reaction field	−121.70	−118.87	−53.89	−51.78	−126.28	−123.53
tot. electrostat energy	−142.82	−148.24	−69.41	−74.23	−149.05	−155.31
Asp122 contribn	−13.69	−21.89	−8.72	−16.01	−14.23	−23.22
models D and D′						
reaction field	−118.28	−115.46	−52.44	−50.35	−123.35	−120.63
tot. electrostat energy	−157.46	−162.89	−72.76	−77.29	−153.53	−159.46
Asp122 contrib	−16.49	−24.56	−10.23	−17.39	−16.48	−25.25

[a] The subscript Asp denotes models C′ and D′, with $\epsilon = 1$ for the CH_2COO^- side chain of Asp 122.

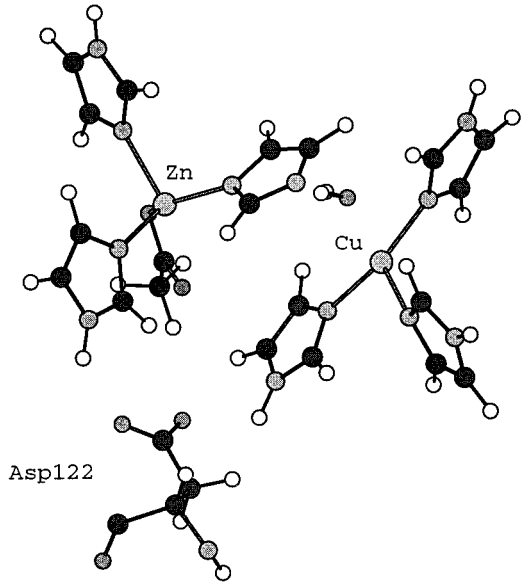

Figure 5. Schematic representation of the active site in the reduced nonprotonated CuZnSOD and the Asp122 residue bridging the His44 and His69 ligands.

energy term. Further, the channel of discrete water molecules contributes significantly, as seen in models C and D.

To further explore the role of Asp122, we carried out calculations for the extended models C′ and D′, which have the same structure as models C and D, respectively, but which extend the $\epsilon = 1$ region to include the CH_2COO^- group of the Asp122 residue. Our motivation for extending the $\epsilon = 1$ region is the observation that Asp122, having a carboxylate group (−1 charge), will interact strongly with the positively charged metal ions and coordinated positive residues (His44 and His69), so that the CH_2COO^- side chain should be immobilized and a vacuum dielectric ($\epsilon = 1$) should be more appropriate than $\epsilon = 4$, which allows for the mobility of polar groups in proteins. The calculated pK_a is more positive in the extended models (Table 6). It is shifted by 1.06 pK_a units in model C′ and by 1.02 pK_a units in model D′. The predicted redox potential is also more positive in the extended models, approaching the experimental value closely in model D′ (calculated value 0.434 eV vs experimental value 0.403 eV). Table 10 gives a detailed breakdown of the reaction-field energy, total electrostatic energy, and the Asp122 contribution to the protein-field energy for models C, C′ and D, D′. The large size of the Asp122 energy and its increasing magnitude when the $\epsilon = 1$ region is extended are evident; the reaction-field term only partially compensates for this effect. The inclusion of the negative charged residue Asp122 in the $\epsilon = 1$ region thus tends to stabilize the protonated reduced structure more than the oxidized structure and, as a result, raises the calculated redox potentials.

4. Conclusions

The four possible intermediates in the coupled electron/proton transfer of the copper zinc superoxide dismutase redox and protonation cycles were geometry optimized. The predicted geometries agree very well with the experimental observations. The calculated minimum-energy reduced geometry has the His61 Nϵ−Cu bond in the active site broken. This bond is elongated during the copper reduction and finally breaks upon protonation of the His61 Nϵ. The His61 Nϵ−Cu bond elongation is due to the antibonding interaction of the Cu d_{z^2}, $d_{x^2-y^2}$ and His61 Nϵ p_z orbitals. The finding that the structural changes during the reduction and protonation of the active site require relatively little energy is consistent with the high reaction rates of superoxide dismutation observed experimentally. The electron which is released from the superoxide onto the copper ion in the first, reductive step is delocalized over the active site. This delocalization of the negative charge makes the copper ion more attractive to the second incoming superoxide molecule. This mechanism involves not only the copper ion and its neighboring ligands but also the zinc ion, which is connected to the Cu ion through the His61 bridge.

The CuZnSOD reduction potential and pK_a were calculated using several models for the extended environment—from aqueous solution to the full protein environment. The calculated reduction potential of the active site in the full protein environment with all X-ray determined water molecules is in very good agreement with experiment.

The predicted pK_a and E°_{redox} probably could be improved by explicitly including geometric and electronic changes of the active site which are induced by the protein/solvent environment.[33,51] However, considering the small difference between the predicted and experimental reduction potential and also the good agreement of calculated and experimental geometries, we conclude that the constraints induced by the full protein environment likely have only a small effect on the active-site geometry. Also, explicit incorporation of Asp122 and Arg141 into the active-site model may improve the result as well.

This study confirms the very complex role of copper zinc superoxide dismutase in the dismutation process. Delicate interactions between the active-site copper and the surrounding ligands are augmented by presence of the His61-bridged zinc ion. Although not directly involved in the catalytic process, the zinc ion participates through its electronic interaction with the active site. Therefore, for an accurate description of the dismutation mechanism, it will be necessary to include both the copper and zinc sites of the complex in the model along with the protein/solvent environment.

Acknowledgment. This work was supported by NIH Grants GM50154 to L.N. and GM45607 to D.B. We wish to thank Drs. D. A. Case, J. A. Tainer, E. Getzoff, D. McRee, and M.

Ludwig for many useful discussions and E. J. Baerends and the Amsterdam group for the use of ADF package. The calculations were carried out on the SGI Power Challenge and Cray T3E computers at The Scripps Research Institute.

Supporting Information Available: Listings of selected geometrical parameters, coordinates, and ESP charges of all clusters calculated in this paper (Tables S1−S7) and diagrams showing various overlays of different cluster geometries (Figures S1−S3). This material is available free of charge on the Internet at http://pubs.acs.org.

IC980730W